Crystallization-induced aggregation of block copolymer micelles: influence of crystallization kinetics on morphology

Adriana M. Mihut · Jérôme J. Crassous · Holger Schmalz · Matthias Ballauff

Abstract We present a systematic investigation of the crystallization and aggregation behavior of a poly(1,2-butadiene)-*block*-poly(ethylene oxide) diblock copolymer (PB-*b*-PEO) in *n*-heptane. *n*-Heptane is a poor solvent for PEO and at 70°C the block copolymer self-assembles into spherical micelles composed of a liquid PEO core and a soluble PB corona. Time- and temperature-dependent light scattering experiments revealed that when crystallization of the PEO cores is induced by cooling, the crystal morphology depends on the crystallization temperature (T_c): Below 30°C, the high nucleation rate of the PEO core dictates the growth of the crystals by a fast aggregation of the micelles into meander-like (branched) structures due to a depletion of the micelles at the growth front. Above 30°C the nucleation rate is diminished and a relatively small crystal growth rate leads to the formation of twisted lamellae as imaged by scanning force microscopy. All data demonstrate that the formation mechanism of the crystals through micellar aggregation is dictated by two competitive effects, namely, by the nucleation and growth of the PEO core.

Keywords Block copolymer · Crystalline micelles · Self-assembly · Selective solvent

A. M. Mihut
Physical Chemistry I, University Bayreuth,
95440 Bayreuth, Germany

J. J. Crassous
Adolphe Merkle Institute, University Fribourg,
1723 Marly, Switzerland

H. Schmalz (✉)
Macromolecular Chemistry II, University Bayreuth,
95440 Bayreuth, Germany
e-mail: holger.schmalz@uni-bayreuth.de

M. Ballauff
Soft Matter and Functional Materials,
Helmholtz-Zentrum Berlin fr Materialien und Energie
GmbH, Glienicker Strasse 100, 14109 Berlin, Germany

M. Ballauff (✉)
Department of Physics, Humboldt University Berlin,
Newtonstr. 15, 12489 Berlin, Germany

Introduction

Self-assembly of crystalline-coil block copolymers in solution has attracted steadily increasing attention during the last years since the resulting morphology may be largely influenced by the crystallizable block. In selective solvents, the insoluble block undergoes chain folding upon crystallization. Thus, the resulting morphology can be viewed as the solvent-soluble corona blocks being grafted on both sides of the lamellar crystalline core [1–3]. The chain-folded crystalline region leads to a dense packing of the amorphous blocks and results in highly stretched tethered chains. The overall shape thus depends on the interplay between the interfacial energy of the crystalline block and the solvent, and the stretching within the amorphous block [4]. Thus, the micellar architecture is strongly influenced by the crystallization conditions, such as temperature [9], and composition of the block copolymers [3, 5–

By changing composition, solvent, and structure of the crystalline block, spherical [7, 11–13], cylindrical [10, 14, 28], and lamellar micelles have been obtained [1, 3, 5, 15, 29]. Recently, Winnik et al. reported the possibility to obtain cylindrical micelles with controlled dimensions and architectures of organometallic block copolymers containing the crystallizable poly-ferrocenyldimethylsilane as one block. These authors, reported the transition from spherical micelles to wormlike, cylindrical or tubular morphologies in non-polar selective solvent [8, 16–18]. Recently, the formation of wormlike micelles was observed in which the corona had undergone a microphase separation in organic media due to crystallization-induced aggregation of triblock terpolymers [14].

In our previous studies, we demonstrated that solutions of poly(butadiene)-*block*-poly(ethylene oxide) in *n*-heptane present a good model system for the study of the interplay between crystallization and aggregation. For a symmetric PB-*b*-PEO block copolymer ($B_{52}EO_{48}^{5,6}$) in *n*-heptane, a fast quenching into liquid nitrogen results in the formation of crystalline micelles retaining the spherical shape present in the molten state at 70°C [19]. If crystallization took place at 30°C, a meander-like structure was formed. Moreover, in the case of a highly asymmetric PB-*b*-PEO block copolymer ($B_{88}EO_{12}^{29,5}$) we observed rod-like micelles [20]. With time these rod-like micelles aggregate and re-crystallize in solution forming long needles. Investigation on a poly(ϵ-caprolactone)-*b*-poly(ethylene oxide) (PCL-*b*-PEO) block copolymer showed that the morphology can be influenced by the crystallization temperature, due to an increased chain folding at lower crystallization temperatures [9].

All previous studies have highlighted the importance of the kinetics of crystallization for the resulting morphology. However, a more detailed investigation of the various factors influencing the micellization of semicrystalline systems is till missing. In this study, we discuss the effect of crystallization kinetics on the morphology formed upon crystallization- induced aggregation of spherical micelles of a symmetric poly(1,2-butadiene)-*block*-poly(ethylene oxide) diblock copolymer ($B_{52}EO_{48}^{5,6}$). The evolution of the size of the aggregates and the kinetics at different crystallization temperatures (T_c) was monitored by static (SLS) and dynamic light scattering (DLS). The resulting crystalline micellar morphologies were imaged by scanning force microscopy (SFM). The combination of the various techniques indicated that the final morphology is directly controlled by T_c: meander-like structures

formed at low T_c, whereas higher T_c lead to the formation of twisted lamellae.

Experimental section

The poly(1,2-butadiene)-*block*-poly(ethylene oxide) diblock copolymer was synthesized via sequential anionic polymerization with a composition given by $B_{52}EO_{48}^{5,6}$ as described elsewhere [22–24]. The subscripts denote the mass fraction in percent and the superscript gives the overall number average molecular weight of the block copolymer in kg/mol. The molecular weights of the PB and PEO blocks are 2.9 and 2.7 kg/mol, respectively. The polydispersity index of the diblock copolymer is 1.02. The samples were prepared from 0.1 wt.% *n*-heptane solutions at different crystallization temperatures for the PEO block.

Differential scanning calorimetry (DSC) measurements on n-heptane solutions of $B_{52}EO_{48}^{5,6}$ (10 wt.%) were performed using a Setaram MicroDSC III in screwcapped stainless aluminum cells. The samples were heated from 25 to 80°C and cooled again to 25°C at a scanning rate of 0.5°C min^{-1}. This cycle was performed three times to check reversibility of the transitions. The samples were kept at 25°C for 60 and 20 min at 80°C.

DLS and SLS were carried out on a ALV compact goniometer system equipped with a He-Ne laser ($\lambda = 632.8$ nm). All measurements were performed on 0.1 wt.% solutions of $B_{52}EO_{48}^{5,6}$ in *n*-heptane at a scattering angle of 90°. The hydrodynamic radius R_H derived from the second cumulant analysis was monitored in two degrees steps with a waiting time of 5 min at each temperature. The samples for the aggregation kinetics were first kept at 70°C during 20 min to erase the thermal history. Then, the samples were quenched in the DLS to different crystallization temperatures. R_H and I/I_0 were monitored every 15 s during 2 h.

The SFM experiments were performed using a Dimension 3,100 M microscope (Veeco Instruments) equipped with a Nanoscope software operated in TappingMode at room temperature. The samples were prepared by spin-coating the 0.1 wt.% $B_{52}EO_{48}^{5,6}$ solution onto freshly cleaned silicon wafers. Scan rates between 0.5–1.0 Hz were used. The crystalline PEO block is much stiffer then the amorphous PB block which allowed us an imaging mode base on a mechanical contrast, complementary to the topographic imaging mode.

Results and discussion

Influence of crystallization temperature (T_c) on the micellar morphology

Recently, we described that crystallization of a poly(1, 2-butadiene)-*block*-poly(ethylene oxide) diblock copolymer ($B_{52}EO_{48}^{5,6}$) in *n*-heptane yielded spherical and meander-like micelles via a fast quenching of the hot solutions (70°C) to 30°C (pathway A), and into liquid nitrogen (pathway B), respectively [19]. The micelles were composed of a crystalline PEO core and a soluble PB corona. The meander structure formed via crystallization-induced aggregation of spherical micelles upon cooling in *n*-heptane. In this study, samples with different thermal histories were prepared in order to investigate the influence of the crystallization conditions on the finally formed morphology. The 0.1 wt.% solutions of $B_{52}EO_{48}^{5,6}$ block copolymer in *n*-heptane were kept at 70°C for 20 min in order to erase any thermal history. Then they were quenched for two hours to 20, 30 and 34°C, respectively. The phase-contrast images clearly confirm the morphological difference between the crystals formed at a distinct T_c (Fig. 1).

Figure 1a–d shows the meander-like morphologies formed in the solutions crystallized at 20 and 30°C, respectively. The width of the meanders was found to be rather uniform, 35 ± 5 nm (Fig. 1a,b) and 40 ± 4 nm (Fig. 1c,d), quantified by measurements from over 50 crystals. The length distribution of the branches is relatively broad, ranging from 35 to 300 nm at $T_c = 30$°C. The branch lengths of the meanders formed at 20°C, is much shorter, varying from 35 to 150 nm.

At 30°C the width of the ribbon-like PEO core has an average value of 20 ± 2 nm, surrounded by an amorphous PB layer of 20 ± 4 nm. The bright areas correspond to the PEO block surrounded by the PB layer as the darker areas indicated in Fig. 1c. The higher contrast of the PEO core is related to a more dense packing of chains in a crystallite compared with the amorphous state. Similar values for the meanders were found in our previous work at this crystallization temperature. The overall thickness measured by SFM from the height images was 16 and 17 nm at 20 and 30°C, respectively. The overall shape of the morphologies resembles that of a fractal growth [25], and is consistent with our previous investigations [19].

In contrast, when the solution is quenched to 34°C (Fig. 1e,f) a change of the crystal morphology is observed which hints to a twisted lamellae. The thickness of the twisted lamellae is 18 nm, which is comparable
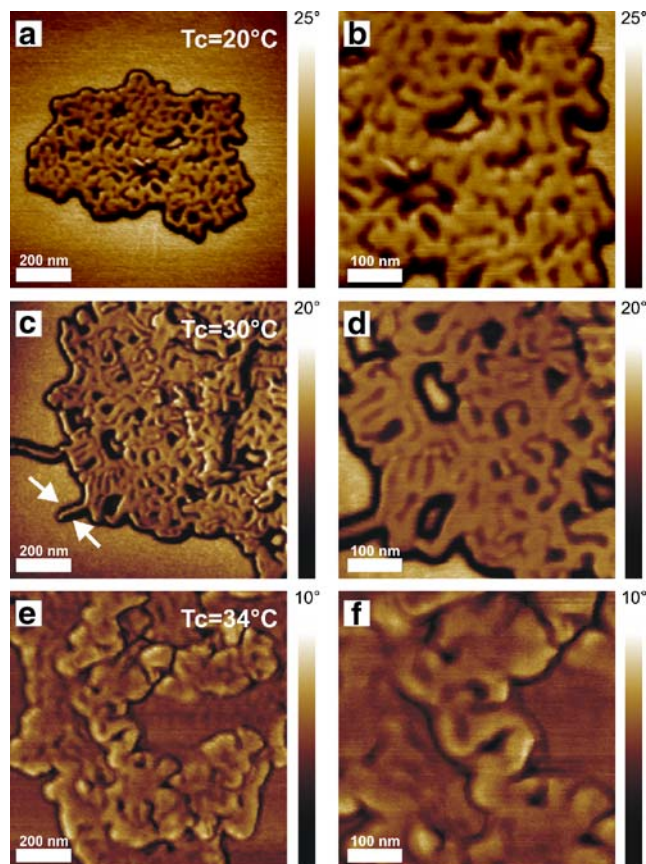
Fig. 1 SFM phase image of $B_{52}EO_{48}^{5,6}$ crystalline micelles from a 0.1 wt.% solution in *n*-heptane after quenching to 20°C (**a**, **b**), 30°C (**c**, **d**) and 34°C (**e**, **f**). The *arrows* point out to the PEO block (*light areas*) and the surrounding PB layer (*darker area*) as can be visualized from the phase contrast difference between the two polymers

with that of the meanders. This shows that there is not change in chain folding due to different quenching temperatures T_c. The average width of the crystals increased to 80 ± 18 nm (quantified from measurements of over 50 crystals) which is twice the size of the crystals formed at lower crystallization temperatures, however the widths are not as uniform as compared to that of the meanders formed at 20 or 30°C.

In thin films, it has been demonstrated that the lamellae thickness increases with crystallization temperature [26, 27]. Large undercooling induced a large chain-folding number, whereas at higher T_c the crystalline polymer chains adopted a fully extended conformation. In addition, investigations on a poly(ϵ-caprolactone)-*b*-poly(ethylene oxide) (PCL-*b*-PEO) block copolymer showed that the extend of chain folding, and as a result the final morphology, can

3
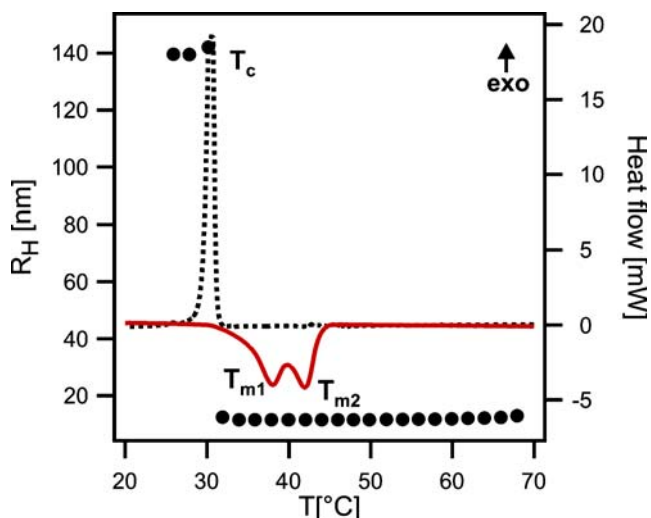
Fig. 2 *Left*: temperature dependence of the hydrodynamic radius (*black circles*) of a 0.1 wt.% solution of $B_{52}EO_{48}^{5.6}$ upon cooling from 70 to 20°C. *Right*: DSC cooling (*black dash line*) and heating scans (*red line*) of a 10 wt.% solution of $B_{52}EO_{48}^{5.6}$ in *n*-heptane

be influenced by the crystallization temperatures [9]. However, in our case the different morphology formed at 34°C does not result from a change in the extend of chain folding, as the thickness of the crystals is comparable to that formed at lower crystallization temperatures. This point will be discussed in more detail in the next section.

Kinetics and mechanism of structure formation

The structure formation upon cooling from 70 to 20°C of the $B_{52}EO_{48}^{5.6}$ *n*-heptane solution has been investigated by DSC and DLS. DSC measurements (Fig. 2 Right) revealed a broaden crystallization transition between 27 and 32°C with a maximum crystallization peak at 30°C. The onset of the crystallization at 30°C was supported by DLS measurements, in which an increase from 12 to 140 nm of the hydrodynamic radius R_H was observed. This is consistent with our previous investigations (Fig. 2 Left) [19]. DSC shows a novel behavior in *n*-heptane solution, which indicated two melting endothermal peaks at 38°C (T_{m_1}) and 42°C (T_{m_2}), whereas in the bulk only a single melting peak at 47°C was observed. Since the double melting endotherms could not be observed in bulk, it is reasonably to conclude that this behavior is induced by the morphology formed in the solution. As the meanders are branched lamellar structures, the first melting endothermal peak from 38°C has to be related with the melting of the less perfect branched points, whereas the second melting peak from 42°C points out to the complete melting of the lamellar units. The DSC heating trace at 70°C is far away from the melting temperature of the crystals, i.e., no thermal history is expected at this temperature.

The kinetics of the crystallization/aggregation process and the size evolution of the aggregates were monitored by measuring the time dependence of the R_H and I/I_0 after fast quenching of the 0.1 wt.%
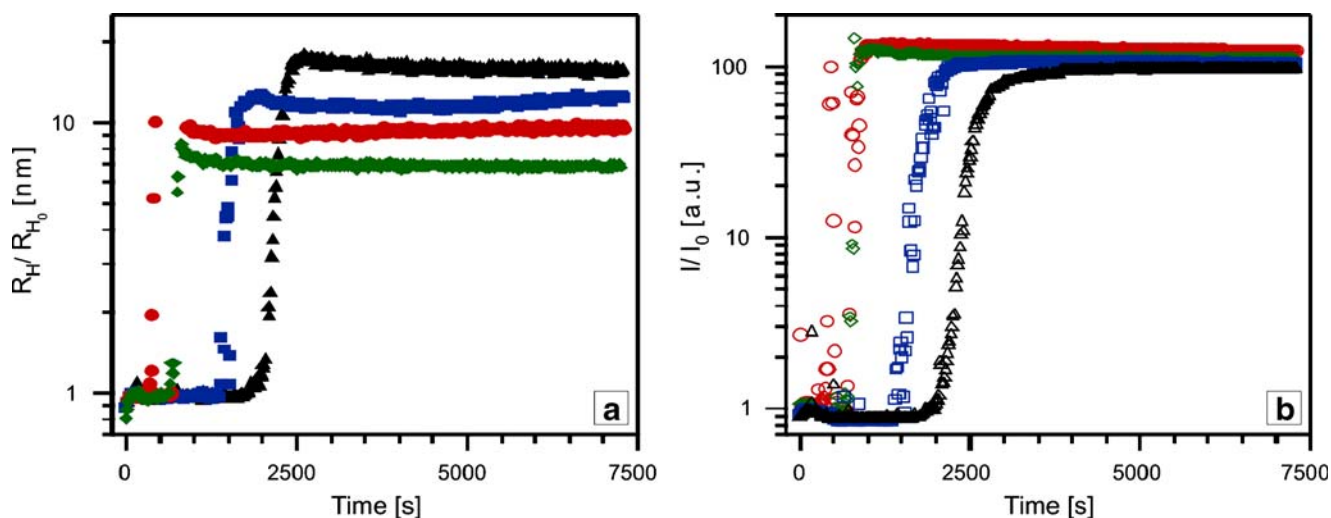
Fig. 3 Evolution of the normalized hydrodynamic radius R_H/R_{H_0} (**a**) and of the normalized scattering intensity I/I_0 (**b**) of 0.1 wt.% solution of $B_{52}EO_{48}^{5.6}$ in *n*-heptane first equilibrated (*blue square*), 30°C (*red circles*) and 20°C (*green diamond*). The *full symbols* correspond to the R_H/R_{H_0} and the *empty symbols* to I/I_0
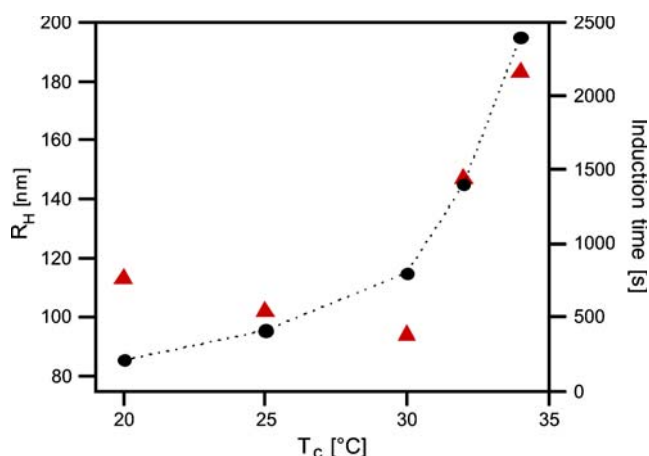
Fig. 4 Dependence of the size of crystalline micelles (*black circles with dash line*) and of the induction time of the primary nucleation process (*red triangle*) on the crystallization temperature (T_c).

solution from 70°C to different T_c directly in the DLS bath. Figure 3 displays the evolution with time of R_H/R_{H_0} and I/I_0 while quenching to different T_c. The R_H and I at time t was normalized to its initial average value R_{H_0} and I_0, respectively before the onset of the crystallization/ aggregation. The R_H retained a constant value of 12 nm when the solution is quenched to 35°C or higher temperatures. At temperatures below 35°C crystallization takes place in the micellar PEO core as monitored by the increase of R_H (Fig. 3a). This indicates rearrangement of micelles and growth into larger structures. An enhancement of the normalized intensity of about two decades marked this transition (Fig. 3b). R_H strongly depends on T_c, i.e., R_H decreases with decreasing T_c, from 195 nm at $T_c = 34$°C to 85 nm at $T_c = 20$°C, respectively (Fig. 4).

A small induction time of the crystallization process was recorded at $T_c \leq 30$°C (only few seconds), whereas at $T_c = 34$°C was delayed with 30 min (Fig. 4). The shortest induction time (400 s) was observed at 30°C, where the maximum of the crystallization exotherm was observed in micro-DSC measurements (Fig. 2). Moreover, the crystallization temperature affects the aggregation time of the micelles, that is, the time until a stable R_H plateau is reached, after the onset of crystallization. The lowest aggregation time was observed at $T_c \leq 30$°C, as 225 and 470 s at 20 and 30°C, respectively. At $T_c > 30$°C, the aggregation time increased to 730 s at 34°C.

The above results suggest the presence of two types of mechanisms in which the crystal growth proceeds in different manners. At $T_c \leq 30$°C, crystallization induced a high nucleation rate in the solution on a narrow

micellar neighbors and fast advancing of the crystallization front in the solution leads to fast depletion of micelles at the growing front. Herein, the crystallization front, therefore the nucleation and growth process, propagates very fast in the solution.

At $T_c > 30$°C, the nucleation rate is lowered and only few nuclei formed at the same time scale in solution. At 34°C, the long induction time of crystallization hinders the detection of an endothermic signal in the DSC, that is, nucleation is too slow at this temperature in order to create nuclei at a slow cooling rate of 0.5°C min^{-1} (see Fig. 2). Due to the reduced number of nuclei/time the growth process is slow and no depletion of micelles occurred at the crystal growth front, as a gradual development of R_H to a stable value was observed (Fig. 3a). Here, the growth process has obviously becomes the step that determines the crystal pattern rather than the nucleation process. It is interesting to note that the crystal morphology is changed concomitantly from meanders (branched lamellae) to twist lamellae at $T_c > 30$°C (Fig. 1).

Conclusion

We can hence conclude that the resulting morphology is controlled by two competitive effects, namely, by the nucleation and growth of the PEO micellar core: At lower T_c, the nucleation rate is high, the crystal growth front is accelerated which results in a meander-like morphology. At higher T_c the nucleation rate is lowered. Thus, the micelles have enough time to reach the growth front of the crystals favoring the formation of twisted lamellae. This procedure allows us to tune morphological structures in dependence on crystallization temperature by change of the growth kinetics.

References

1. Lotz B, Kovacs AJ (1966) Kolloid-Z Z Polym 209:97–114
2. Lotz B, Kovacs AJ, Bassett GA, Keller A (1966) Kolloid-Z Z Polym 209:115–128
3. Lin EK, Gast AP (1996) Macromolecules 29:4432–4441

5. Richter D, Schneiders D, Monkenbusch M, Willner L, Fetters LJ, Huang JS, Lin M, Mortensen K, Farago B (1997) Macromolecules 30:1053–1068
6. Massey JA, Temple K, Cao L, Rharbi Y, Raez J, Winnik MA, Manners IJ (2000) Am Chem Soc 122:11577–11584
7. Xu JT, Fairclough JPA, Mai SM, Ryan AJJ (2003) Mater Chem 13:2740–2748
8. Shen L, Wang H, Guerin G, Wu C, Manners I, Winnik M (2008) Macromolecules 41:4380–4389
9. Du Z-X, Xu J-T, Fan Z-Q (2008) Macromol Rapid Commun 29:467–471
10. Du Z-X, Xu J-T, Fan Z-Q (2007) Macromolecules 40:7633–7637
11. Fu J, Luan B, Yu X, Cong Y, Li J, Pan C, Han Y, Yang Y, Li B (2004) Macromolecules 37:976–986
12. Xu JT, Jin W, Liang GD, Fan ZQ (2005) Polymer 46:1709–1716
13. Cao L, Manners I, Winnik MA (2002) Macromolecules 35:8258–8260
14. Schmalz H, Schmelz J, Drechsler M, Yuan J, Walther A, Schweimer K, Mihut AM (2008) Macromolecules 41:3235–3242
15. Zheng JX, Xiong HM, Chen WY, Lee KM, Van Horn RM, Quirk RP, Lotz B, Thomas EL, Shi AC, Cheng SZD (2006) Macromolecules 39:641–650
16. Guerin G, Raez J, Manners I, Winnik MA (2005) Macromolecules 38:7819–7827
17. Raez J, Barjovanu R, Massey JA, Winnik MA, Manners I (2000) Angew Chem Int Ed 39:3862–3865
18. Raez J, Tomba JP, Manners I, Winnik MAJ (2003) Am Chem Soc 125:9546–9547
19. Mihut AM, Chiche A, Drechsler M, Schmalz H, Cola ED, Krausch G, Ballauff M (2009) Soft Matter 5:208–213
20. Mihut AM, Drechsler M, Möller M, Ballauff M (2009) Macromol Rapid Commun. doi:10.1002/marc.200900571
21. Xu J-T, Fairclough JPA, Mai S-M, Ryan AJJ (2003) Mater Chem 13:2740–2748
22. Schmalz H, Lanzendörfer MG, Abetz V, Müller AHE (2003) Macromol Chem Phys 204:1056–1071
23. Schmalz H, Knoll A, Müller AJ, Abetz V (2002) Macromolecules 35:10004–10013
24. Castillo RV, Arnal ML, Müller AJ, Hamley IW, Castelletto V, Schmalz H, Abetz V (2004) Macromolecules 41:879–889
25. Reiter G, Hörner P, Hurtrez G, Riess G, Sommer JU, Joanny JFJ (1998) Surf Sci Technol 14:93–103
26. Sommer J-U, Reiter GJ (2000) Chem Phys 112:4384–4393
27. Reiter G, Sommer J-U (2000) J Chem Phys 112:4376–4383
28. Lazzari M, Scalarone D, Vazquez-Vazquez C, Lopez-Quintela MA (2008) Macromol Rapid Commun 29:352–357
29. Gädt T, Ieong NS, Cambridge G, Winnik MA, Manners I (2009) Nat Mater 8:144–150
30. Arlie J, Spegt P, Skoulios A (1967) Makromol Chem 104:212–229
31. Kovacs A, Straupe C (1980) J Cryst Growth 48:210–226